



# Affective information modulates slow-wave- and arousal-like responses during NREM sleep



Demetrio Grollero <sup>1,2</sup>, Damiana Bergamo <sup>1,3</sup>, Alessandra Federici <sup>1</sup>, Ruggero Basanisi <sup>1</sup>, Davide Bottari <sup>1</sup>, Monica Betta <sup>1</sup> & Giulio Bernardi <sup>1</sup>

Sleep is characterized by relative disconnection from the external environment and prompt reversibility in response to salient stimuli. During non-rapid eye movement (NREM) sleep, reactive electroencephalographic (EEG) slow waves (K-complexes, KC) are thought to both suppress the processing of external stimuli and open ‘sentinel’ windows during which further relevant inputs may be tracked. However, the extent to which a stimulus’s relevance modulates the KC-related response remains unclear. Here, we investigated the impact of emotional information in human vocal bursts on KC and post-KC activity. Twenty-five young adults were presented with vocal bursts conveying negative, neutral, and positive emotions. We found that affective content influenced the rate, amplitude, and cortical distribution of KCs, as well as post-KC high-frequency activity. These results indicate that KCs are not all-or-none responses and that salient information is not entirely ‘quenched’ by KCs. These insights offer new perspectives on how sleep continuity and reversibility are regulated.

Sleep is a reversible, homeostatically regulated physiological state characterized by behavioral quiescence and reduced responsiveness to environmental stimuli. Sleeping animals are unable to engage in productive behaviors such as foraging, eating, drinking, or mate-seeking and are exposed to potential threats in the surrounding environment<sup>1,2</sup>. Viewed through an evolutionary lens, such a peculiar condition appears biologically plausible only under the assumption that it must serve at least one vital function. Indeed, evidence indicates that sleep actually controls many essential processes, including, amongst others, learning and memory consolidation, emotional regulation, and the maintenance of cognitive and behavioral efficiency<sup>3</sup>. Notably, these functions are negatively affected by sleep fragmentation due to frequent arousals or awakenings (e.g., <sup>4–6</sup>). In this light, functional mechanisms able to sustain sleep continuity in the face of irrelevant environmental stimuli and favor reactivity to biologically relevant ones may have obvious evolutionary advantages<sup>7</sup>.

K-complexes (KCs; <2 Hz) are hallmark features of non-rapid-eye-movement (NREM) sleep, traditionally thought to regulate sensory disconnection by balancing sleep-protective and reactive functions<sup>8</sup>. In particular, KCs have been suggested to exhibit a “Janus-faced” nature, acting both as stabilizers of sleep and as potential facilitators of arousal<sup>9</sup>. Like spontaneous slow waves of NREM sleep, KCs reflect the coordinated occurrence of neuronal off periods (silence) between on periods of active firing<sup>10</sup>. However, unlike typical slow waves, KCs can be triggered

by external sensory stimuli and tend to be larger and more widespread, likely due to efficient bottom-up synchronization driven by arousal-related structures<sup>11,12</sup>. Previous work suggested that KCs may represent stereotyped, all-or-none responses whose shape and topography remain largely independent of stimulus salience or intensity<sup>13</sup>. Due to their nature of widely synchronized neuronal silencing events, KCs are believed to play a key role in “quenching” incoming sensory information, helping to preserve sleep continuity<sup>14,15</sup>. However, KCs also exhibit a reactive component: they are often followed by increased high-frequency activity and/or microarousals, suggesting a transient shift toward a “sentinel mode” that may enhance the detection and processing of subsequent stimuli<sup>16–18</sup>. Accordingly, KCs have been suggested to first dampen incoming sensory input before briefly promoting environmental monitoring<sup>19–21</sup>. Despite compelling evidence for this dual function, it remains unclear how stimulus salience influences the protective versus reactive components of KCs and, consequently, the regulation of sensory disconnection during sleep.

Interestingly, social communication stimuli, especially those with emotional content, hold unique relevance for human beings. Indeed, both verbal and non-verbal affective cues may convey information of high importance for awake and sleeping individuals alike, including the occurrence of potentially dangerous or favorable events. Evolutionarily, one would expect selective pressures to favor adaptations that prioritize the processing of such relevant communicative signals. Consistent with this, prior research

<sup>1</sup>MoMiLab Research Unit, IMT School for Advanced Studies Lucca, Lucca, Italy. <sup>2</sup>Department of Experimental and Clinical Medicine, Neurological Clinic, Marche Polytechnic University, Ancona, Italy. <sup>3</sup>Department of General Psychology, University of Padova, Padova, Italy. e-mail: [giulio.bernardi@imtlucca.it](mailto:giulio.bernardi@imtlucca.it)

demonstrated that certain stimuli - such as hearing one's own name (vs. someone else's name;<sup>19,22,23</sup>), unfamiliar voices (vs. familiar voices;<sup>18,19</sup> or voices characterized by specific emotional prosody (vs. neutral voices;<sup>24-26</sup>) - elicit distinctive EEG responses during sleep. However, most studies investigating the influence of affective stimuli on sleep either excluded stimulation trials containing KCs (e.g.,<sup>25</sup>) or did not analyze them separately from trials without KCs (e.g.,<sup>26</sup>). The few studies focusing on KCs typically employed a small number of stimuli that were repeatedly presented throughout the night and across sleep stages. However, the ability of a stimulus to evoke KCs is known to decrease with repeated exposure<sup>18,27</sup>. Furthermore, most studies have focused primarily on negative (vs. neutral) emotional content, leaving the broader generalizability of their findings open to question.

Building on these considerations, the present study aimed to investigate if, and to what degree, KC-related brain responses are modulated by the emotional valence of non-verbal human vocalizations (*vocal bursts*). To optimize the induction of stimulus-dependent KCs, we employed an experimental protocol in which distinct affective stimuli were presented only once and with long inter-stimulus intervals, thereby minimizing the risk of habituation and learning. Additionally, stimuli were delivered exclusively during NREM sleep to prevent cross-stage interactions. Vocal bursts were chosen over verbal stimuli as they represent an elementary, phylogenetically older form of emotional expression<sup>28-32</sup>. We applied a range of analytical techniques to characterize KC-related responses, including event-related potentials (ERPs), topographic and source-level analyses of specific KC subcomponents, time-frequency decomposition, and assessments of relative signal power changes. We hypothesized that emotionally salient stimuli, signaling potential threats or positive events in the sleeper's environment, would elicit functional responses with enhanced high-frequency, arousal-like components, reflecting a temporary shift toward a brain "sentinel mode."

Our results indicate that the occurrence, morphology, and spatial distribution of KCs, as well as post-KC neural dynamics, are modulated by the emotional salience of incoming stimuli. These results challenge the traditional view of KCs as uniform, all-or-none responses and instead suggest that they are embedded within a multiphasic, adaptive process. This

process may allow the brain to transiently increase environmental awareness without fully disrupting sleep, thereby supporting a dynamic balance between sensory disconnection and responsiveness to salient external cues.

## Results

### Processing of stimulus valence during wakefulness

Negative, neutral, positive emotional vocal burst stimuli employed in the present study were selected according to affective ratings provided by 12 healthy adult volunteers (Fig. 1a), as detailed in previous work<sup>33</sup>. Notably, a-posteriori analyses revealed strong agreement between the ratings used for stimulus selection and those provided by participants in the current experiment, with Spearman's rho values indicating high correlation for both valence (rho = 0.96; adjusted  $R^2 = 0.94$ ) and arousal (rho = 0.86; adjusted  $R^2 = 0.73$ ; see Supplementary Fig. 1).

Stimulus-related EEG responses during wakefulness, measured by Global Field Potentials (GFP), exhibited significant differences across the three valence classes within the time window of 238 to 312 ms following stimulus onset ( $p = 0.008$ , rmANOVA with cluster-mass correction; cluster size = 38 time-points; Fig. 2). Post-hoc comparisons revealed that both negative and positive stimuli were associated with a stronger GFP response relative to neutral ones ( $p < 0.01$ , paired  $t$ -tests; also see Supplementary Fig. 2). No difference was observed between negative and positive stimuli.

### Proportion and amplitude of evoked KCs

Overall,  $84.34 \pm 7.83\%$  of the stimuli were associated with an evoked KC (Fig. 3). Stimuli with a positive valence had a lower probability of being followed by a KC relative to both neutral ( $p = 0.002$ ; Hedges'  $|g| = 0.482$ , 95% CI = [0.799; 0.248]) and negative ( $p = 0.033$ ;  $|g| = 0.364$ , CI = [0.723; 0.068]) stimuli (rmANOVA,  $F(2,48) = 5.07$ ;  $p = 0.009$ , Fig. 3b). The peak-to-peak amplitude of evoked KCs was significantly larger for negative ( $p = 0.002$ ;  $|g| = 0.207$ , CI [0.103; 0.344]) and positive ( $p = 0.017$ ;  $|g| = 0.134$ , CI = [0.027; 0.276]) stimuli relative to neutral ones (rmANOVA  $F(2,48) = 6.66$ ;  $p = 0.003$ ; Fig. 3c). No significant amplitude difference emerged between negative and positive stimuli ( $p = 0.195$ ).

Of note, we observed in the ERP plot for stimuli that did not evoke KCs a negative deflection around the time of stimulus presentation (Fig. 3a).

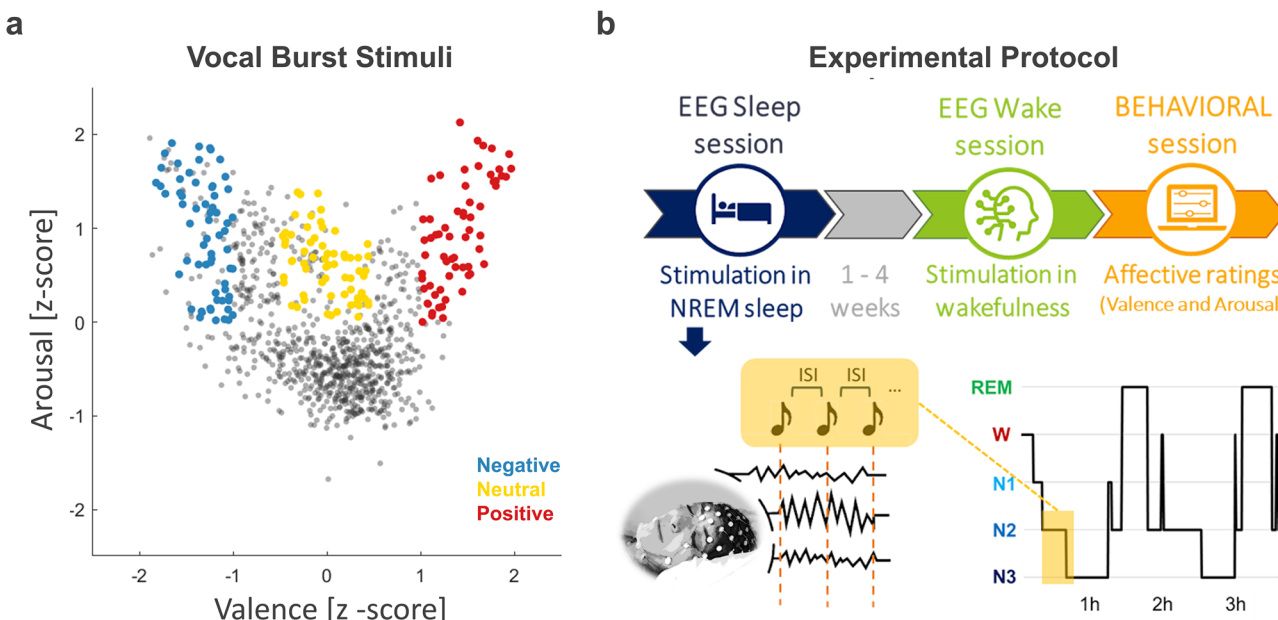


**Fig. 1 | Experimental procedures.** **a** Each dot represents a stimulus from the original full pool ( $n = 1008$  stimuli) plotted with respect to its z-scored valence (x-axis) and arousal (y-axis). Colored dots represent the selected stimuli for negative (blue), neutral (yellow), and positive (red) valence. **b** Experimental paradigm. Each participant completed an overnight EEG session and a

wakefulness session, the latter including an EEG recording during stimulus presentation and an affective rating task. Vocal burst stimuli were presented in random order during NREM sleep and wakefulness experimental sessions. The photo used in this figure was reproduced and modified with permission from the author, Agnese Morganti.

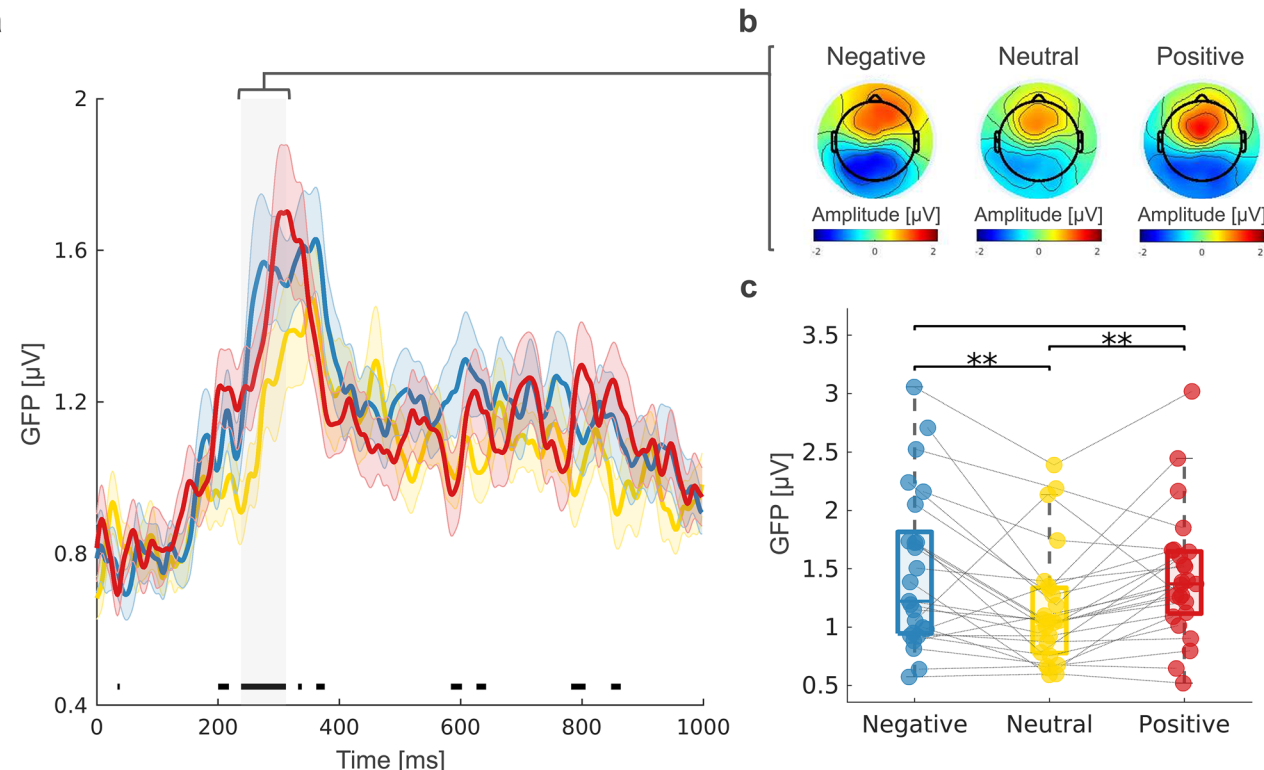


**Fig. 2 | Stimulus-dependent brain activity changes during wakefulness.** **a** The Global Field Potential (GFP) responses are shown as average  $\pm$  standard error of the mean (SEM), with different colors for negative (blue), neutral (yellow), and positive (red) valence stimuli. Time 0 corresponds to stimulus onset. The dark bars at the bottom of the plot indicate uncorrected effects with  $p < 0.05$  (rmANOVA). The gray shaded area corresponds to significant effects surviving after correction for multiple

comparisons ( $p < 0.05$ , corrected). **b** Topographic distribution of mean EEG voltages across significant timepoints. **c** Post-hoc comparisons based on mean GFP values across significant timepoints, each dot represents a distinct participant ( $n = 25$ ).  $^*p < 0.05$ ,  $^{**}p < 0.01$ ,  $^{***}p < 0.001$ . Box-plots whiskers represent  $\pm 1.5$  IQR from Q1/Q3.

Based on this, we hypothesized that spontaneous slow waves occurring around stimulus onset may have prevented the appearance of evoked KCs. To test this hypothesis, we identified spontaneous slow waves that occurred between  $-0.5$  and  $+0.25$  s relative to stimulus onset. We found that the slow-wave occurrence probability around stimulus onset did not significantly differ across the three valence classes (rmANOVA,  $F(2,48) = 1.27$ ;  $p = 0.291$ ). On the other hand, trials lacking an evoked KC more often coincided with the occurrence of spontaneous slow waves around the time of stimulus presentation relative to trials with an evoked KC regardless of stimulus valence ( $60 \pm 22\%$  vs.  $29 \pm 13\%$ ;  $p < 0.001$ ; Fig. 4a). Therefore, we next compared the properties of spontaneous slow waves across trials associated and not associated with a subsequent KC. We found that spontaneous slow waves did not differ in terms of overall amplitude (Fig. 4b), but showed instead significant differences in topographic distribution (Fig. 4c). Specifically, slow waves presenting a stronger involvement of bilateral temporal and parietal electrodes were less likely to be followed by an evoked KC (paired-sample  $t$ -test, nonparametric cluster-based permutation tests with 5000 iterations, corrected  $p < 0.5$ ; cluster size = 27).

#### Topographic analysis of evoked KCs

In addition to the main negative component (N550), KCs are typically characterized by early (P200) and late (P900) positive peaks (Supplementary Fig. 3). Previous work suggested that the early components of the KC may reflect a bottom-up excitatory cortical response holding information about the physical characteristics of the stimulus, while late KC components mainly reflect cortical activity suppression and cortico-thalamic recursive interactions<sup>14,15</sup>. Here, we found no significant impact of stimulus valence on the topographic distribution of the P200 component (rmANOVA,  $p > 0.05$ ; Fig. 5). Instead, significant effects were found for both the N550 and the P900 components. Specifically, we found for the

N550 a significant effect of valence spanning centro-frontal and lateral electrodes on both the right and left sides (rmANOVA,  $p = 0.003$ ; cluster size = 39). Post-hoc tests showed that these electrodes were associated with a stronger involvement for negative relative to neutral stimuli ( $p < 0.001$ ; median  $|g| = 0.183$ , CI = [0.091; 0.321]). A follow-up source-modeling analysis showed that differences in the negative component of the KC between negative and neutral stimuli mainly involved a set of brain areas distributed bilaterally in the superior/middle temporal region, orbito/ventrolateral frontal region, and occipital region ( $q < 0.05$  FDR corrected; Fig. 6a).

No significant differences were found between positive stimuli and either negative or neutral stimuli. For P900, we found a centro-frontal effect mainly extending to left-side scalp electrodes (rmANOVA,  $p = 0.006$ ; cluster size = 32). Post-hoc tests revealed in these electrodes a stronger involvement for both negative ( $p < 0.001$ ; median  $|g| = 0.381$ , CI = [0.107; 0.742]) and positive ( $p < 0.05$ ; median  $|g| = 0.202$ , CI = [0.107; 0.742]) stimuli relative to neutral ones. Source-level analyses showed that differences between positive and neutral stimuli in the late positive component of the KC involved the caudal portion of the middle frontal area and the posterior cingulate bilaterally, the left pre- and post-central areas, and the right lateral orbitofrontal cortex and anterior cingulate areas (Fig. 6b). Source-level differences between negative and neutral stimuli emerged in the bilateral cingulate and parahippocampal areas bilaterally, left superior-temporal areas, left pre-/post-central areas, and right medial-occipital and inferior-temporal areas. No significant differences were found between negative and positive stimuli.

#### Brain activity changes time-locked to evoked KCs

We next used time-frequency decomposition to examine brain activity changes around and after evoked KCs. We observed significant differences

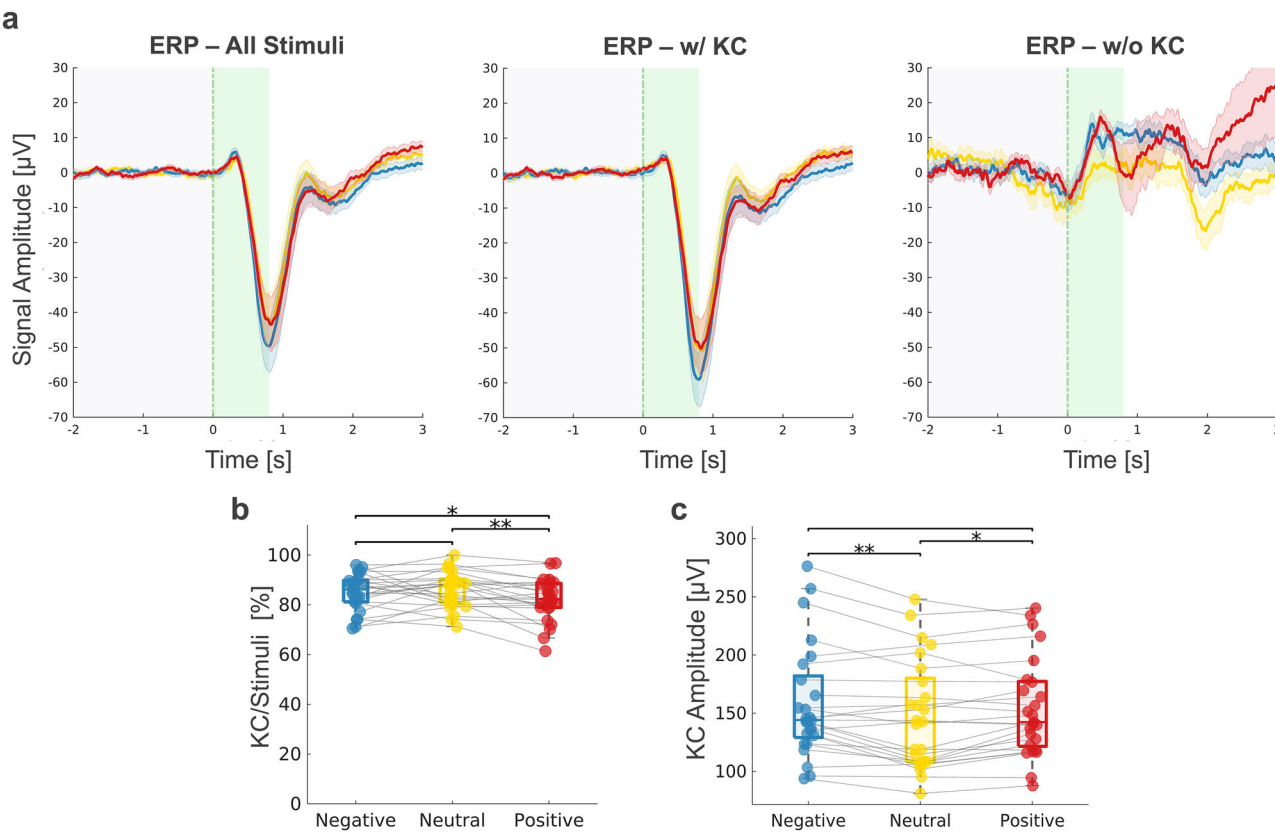


**Fig. 3 | Evoked KCs.** **a** From left to right, the panel shows the ERPs computed from all stimuli, the ERPs computed only from stimuli followed by a KC, and the ERPs computed only from stimuli that did not lead to a KC. The green shaded area marks the time between stimulus onset and offset, while the gray shaded area marks the window used for baseline correction. The ERPs are shown as average  $\pm$  standard error of the mean (SEM), with different colors for negative (blue), neutral (yellow), and positive (red) valence stimuli. For display purposes, the plotted signals were detrended using robust detrend and low-pass filtered at 45 Hz. **b** The boxplots show the ratio between evoked KCs and administered stimuli for each valence class. **c** The boxplots show the mean peak-to-peak amplitude of evoked KCs for each valence class. In **b** and **c**, each dot represents a distinct participant ( $n = 25$ ). \* $p < 0.05$ , \*\* $p < 0.01$ , \*\*\* $p < 0.001$ . Box-plots whiskers represent  $\pm 1.5$  IQR from Q1/Q3.

and positive (red) valence stimuli. For display purposes, the plotted signals were detrended using robust detrend and low-pass filtered at 45 Hz. **b** The boxplots show the ratio between evoked KCs and administered stimuli for each valence class. **c** The boxplots show the mean peak-to-peak amplitude of evoked KCs for each valence class. In **b** and **c**, each dot represents a distinct participant ( $n = 25$ ). \* $p < 0.05$ , \*\* $p < 0.01$ , \*\*\* $p < 0.001$ . Box-plots whiskers represent  $\pm 1.5$  IQR from Q1/Q3.

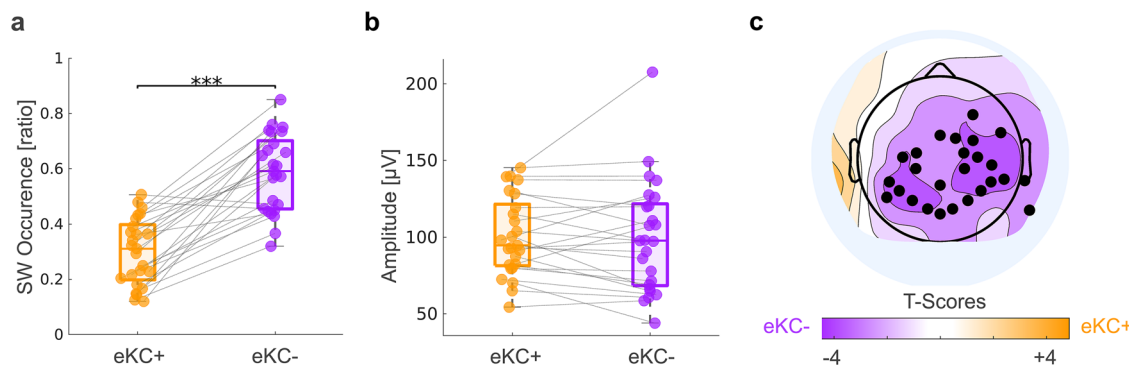


**Fig. 4 | Effect of spontaneous slow waves on evoked KCs.** **a** The boxplots show the percentage of spontaneous slow waves detected around the onset of stimulus presentation with respect to the total number of trials with evoked KCs (KC+) or no detected KCs (KC-). **b** The boxplots show the mean amplitude of spontaneous slow waves detected around the onset of stimulus presentation for trials with evoked KCs. **c** Difference in topographic scalp involvement of slow waves detected around stimulus onset between trials with evoked KCs (orange) and no detected KCs (purple). Black dots mark significant effects ( $p < 0.05$ , cluster-mass correction). In **a**, **b**, each dot represents a distinct participant ( $n = 25$ ). \* $p < 0.05$ , \*\* $p < 0.01$ , \*\*\* $p < 0.001$ . Box-plots whiskers represent  $\pm 1.5$  IQR from Q1/Q3.

or no detected KCs. **c** Difference in topographic scalp involvement of slow waves detected around stimulus onset between trials with evoked KCs (orange) and no detected KCs (purple). Black dots mark significant effects ( $p < 0.05$ , cluster-mass correction). In **a**, **b**, each dot represents a distinct participant ( $n = 25$ ). \* $p < 0.05$ , \*\* $p < 0.01$ , \*\*\* $p < 0.001$ . Box-plots whiskers represent  $\pm 1.5$  IQR from Q1/Q3.

between stimuli with both negative and positive valence in comparison to neutral stimuli ( $p < 0.05$ , cluster-based correction; Fig. 7), while no significant differences emerged between the negative and positive valence categories. In particular, we found that negative and positive valence stimuli were associated with increases in the alpha-sigma range (8–16 Hz) between  $-100$  and  $+500$  ms relative to the negative peak of the KC, and in beta activity (20–30 Hz) between  $100$  and  $600$  ms after the KC negative peak. These changes were mainly observed in bilateral temporal and parietal

electrodes but also extended to central and frontal ones (see Supplementary Figs. 4 and 5).

#### Brain activity changes after evoked KCs

Finally, we investigated potential changes in EEG activity in the few seconds after a KC (from 2 to 6 s after the KC negative peak), focusing on delta, alpha, and beta signal power<sup>11</sup>. We found no significant effects of valence for delta and alpha power (Supplementary Fig. 6). Instead, a significant effect was

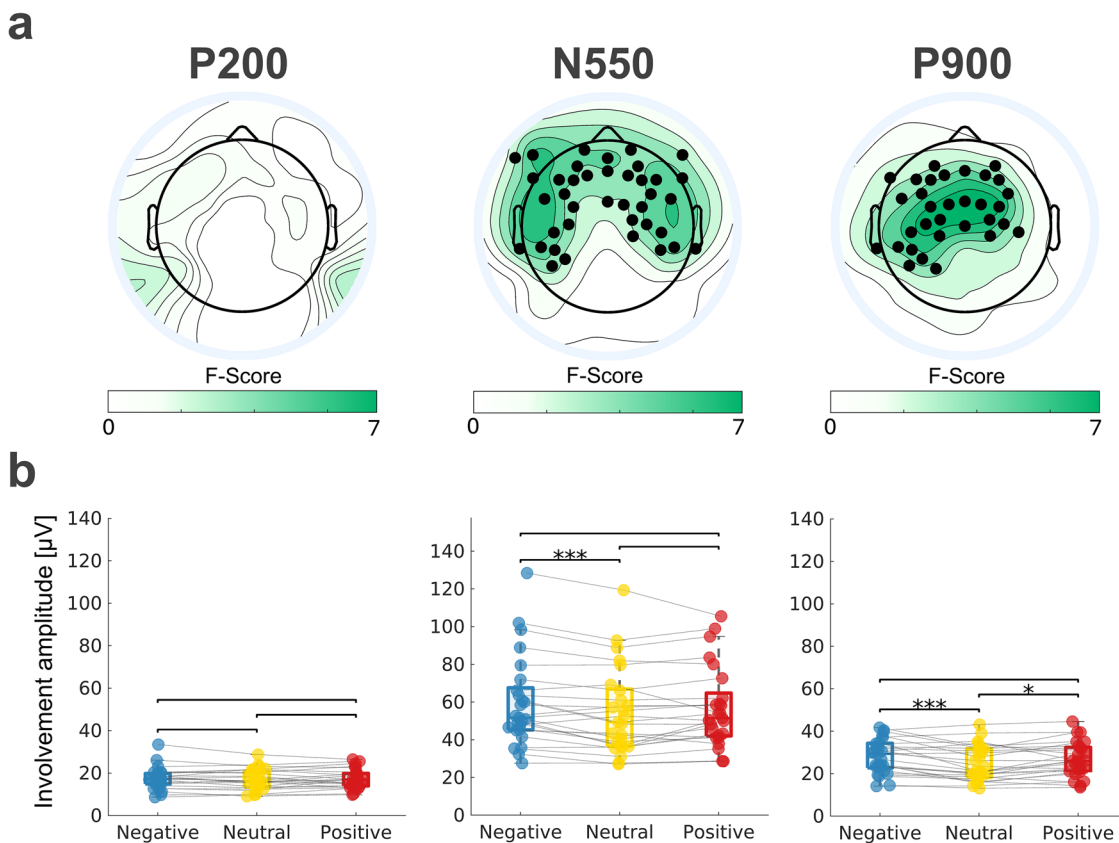


**Fig. 5 | Results of the topographic analyses for distinct components of the KC.** a From left to right, the panel shows the results of the rmANOVA for P200, N550, and P900 components. Black dots mark electrodes showing a significant effect with  $p < 0.05$ , cluster-mass correction. b From left to right, the panel shows the post-hoc comparisons for P200, N550, and P900 components. Each dot represents the average

value across significant electrodes shown in a for each participant ( $n = 25$ ). P200 values were obtained computing the average across all electrodes as no significant effects were observed in the topographic analysis.  $*p < 0.05$ ,  $**p < 0.01$ ,  $***p < 0.001$ . Box-plots whiskers represent  $\pm 1.5$  IQR from Q1/Q3.

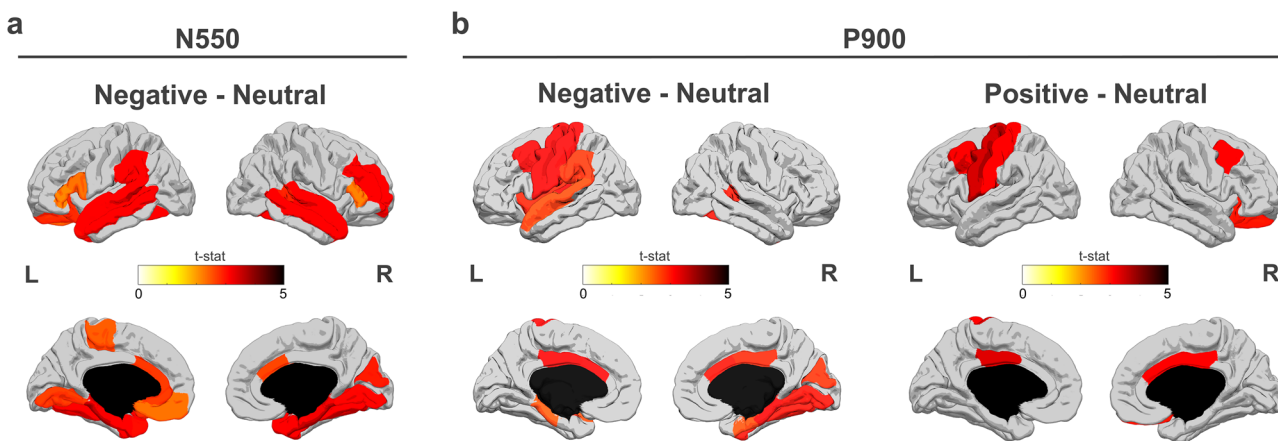


**Fig. 6 | Source modeling analysis of the N550 and P900 KC components.** a Significant differences in the N550 KC component between negative and neutral stimuli (t-score;  $q < 0.05$ , FDR correction). b Significant differences in the P900 KC

component between negative and neutral stimuli (left), and between positive and neutral stimuli (right). Medial structures depicted in black were not modeled and tested.

observed for beta power in a cluster of right-lateralized temporo-parietal electrodes ( $p < 0.05$ , cluster-mass correction; Fig. 8b). Post-hoc analyses revealed a stronger beta increase for positive relative to both neutral ( $p < 0.01$ ) and negative ( $p < 0.05$ ) stimuli (Fig. 8c). A tendency toward higher beta activity for negative relative to neutral stimuli was also observed ( $p < 0.1$ ). This difference reached significance after the removal of two outliers in the neutral condition ( $p < 0.05$ ).

A source-level contrast between positive and neutral stimuli for beta power revealed significant differences ( $q < 0.05$ , FDR correction) in bilateral

prefrontal and orbitofrontal areas, anterior cingulate cortex, inferior, medial, and superior temporal cortices, and in the left precuneus and superior parietal cortex (Fig. 8e).

## Discussion

The present study investigated how affective information embedded into human vocalizations influences the generation and properties of stimulus-related KCs and post-KC brain activity during NREM sleep. Our results showed that vocal bursts with a positive or negative valence trigger KCs with

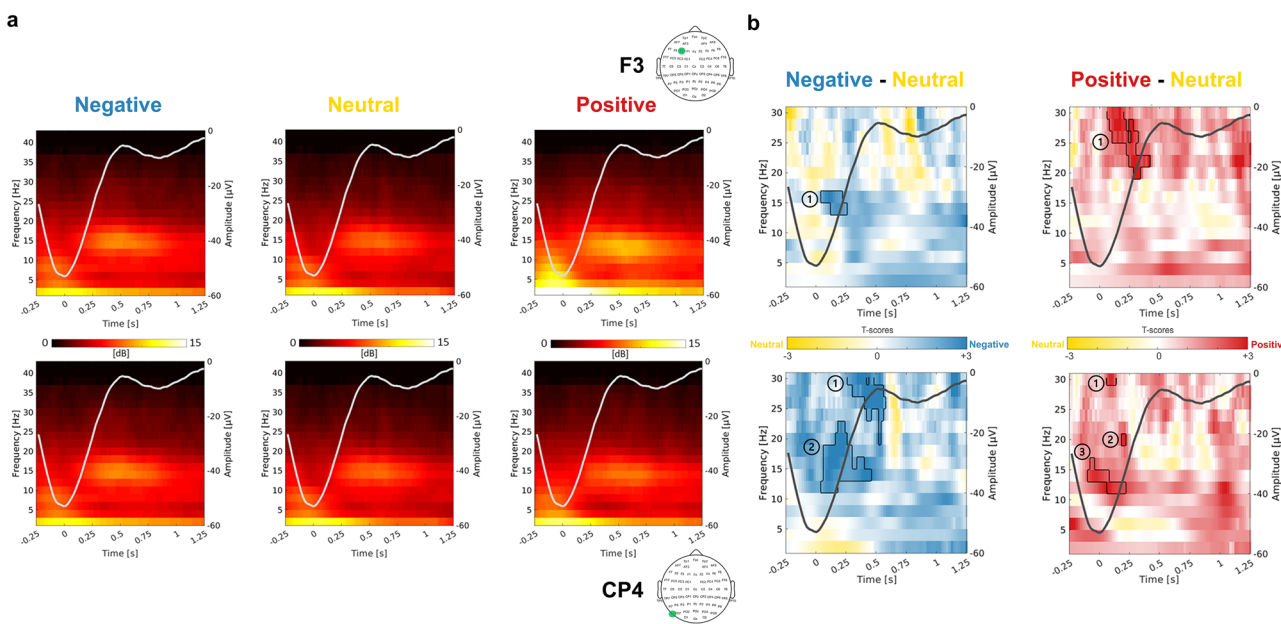


**Fig. 7 | Time-frequency analysis.** Brain activity changes associated with the occurrence of KCs were assessed using a time-frequency analysis time-locked to the KC negative peak. The plots in the top panels refer to a frontal electrode (F3), while the bottom panels refer to a centro-parietal electrode (CP4). **a** Time-frequency signal decomposition for negative, neutral, and positive stimuli. The mean KC response (scaled to the right y-axis) is superimposed on the time-frequency results to better illustrate the relationship between the KC phase and power changes. **b** Significant differences for the contrasts between negative and neutral stimuli (left), and between

positive and neutral stimuli (right) in two representative electrodes. Dark contours mark significant differences at  $p < 0.05$ , corrected. For each significant cluster, we calculated the percent power difference relative to the neutral condition (mean  $\pm$  SEM). F3 electrode: negative vs. neutral, cluster 1 =  $17.15 \pm 5.44\%$ ; positive vs. neutral, cluster 1 =  $31.39 \pm 7.76\%$ . CP4 electrode: negative vs. neutral, cluster 1 =  $40.57 \pm 10.06\%$ , cluster 2 =  $24.12 \pm 7.47\%$ ; positive vs. neutral, cluster 1 =  $74.71 \pm 50.83\%$ , cluster 2 =  $46.24 \pm 21.95\%$ , cluster 3 =  $27.27 \pm 7.60\%$ .

distinctive characteristics relative to neutral stimuli, consistent with a preserved encoding of affective valence during NREM sleep even during and after KCs, and in contrast with the common view of KCs as *all-or-none* events. Given the hypothesized sleep-preserving and reactive roles of KCs, these different responses may indicate a higher probability for affective stimuli to induce a shift of the sleeping brain toward a “*sentinel mode*,” in which the processing of external stimuli is temporarily enhanced.

### Stimulus valence influences both the occurrence and morphology of KCs

The rate at which external stimuli trigger KCs typically varies in the literature between 10% and 50% (e.g.,<sup>14,34</sup>) and is known to depend on several factors, including the sensory modality, the salience, and the repetition rate of the stimuli, as well as interindividual differences among sleepers. In the present study, over 80% of the stimuli elicited a KC, a rate appreciably higher than those reported in previous studies using human verbal or nonverbal vocal stimuli (e.g.,<sup>18,23</sup>). This higher rate is likely attributable to key differences in our stimulation protocol. Indeed, unlike most prior investigations, we employed long inter-stimulus intervals ( $\geq 8$ s) and avoided stimulus repetition. While this design limited our ability to systematically assess changes in brain responsiveness across different sleep cycles or throughout the night, it allowed us to isolate the effects of stimulus valence on KCs more effectively. By reducing potential confounds such as refractory periods, habituation, and stimulus learning, this approach ensured that the observed differences in KC responses were not driven by adaptation effects but rather by the intrinsic affective properties of the stimuli. This approach allowed us to isolate the effect of valence on KCs, minimizing the possible impact of confounding factors such as those related to refractory periods, habituation, and stimulus learning.

Our results revealed that vocal bursts with a positive valence had a lower probability of triggering a KC compared to both neutral and negative stimuli. This finding suggests that positive stimuli may be identified by the sleeping brain very early during stimulus processing, potentially due to distinctive low-level features. The lower likelihood of KC occurrence might

indicate that the brain recognizes positive affective stimuli as less salient or less likely to require an alerting response than negative or neutral stimuli<sup>18,35</sup>. However, this observation partially contrasts with other findings in this study, which demonstrate stronger high-frequency increases following positive stimuli compared to other valence classes (see below). One possible explanation for this discrepancy is that while positive stimuli may be interpreted as signaling a low risk for the sleeper, they could also serve as social or motivationally relevant cues, prompting the brain to allocate cognitive resources toward detecting potential advantageous opportunities in the surroundings. According to this view, positive vocal bursts may inherently carry a lower sleep-disruptive potential compared to threatening or negative stimuli, thereby reducing the need for strong KC-mediated suppression. Although positive stimuli may have lower arousal potential, they could be more effective than negative stimuli in inducing a sentinel mode state, owing to the engagement of reward-processing systems. This dual-pathway model could reconcile the apparent contradiction between reduced KCs and enhanced high-frequency responses, emphasizing the brain’s ability to differentially prioritize stimuli based on their affective and motivational significance.

The question of whether the amplitude and shape of K-complexes (KCs) can be modulated by the salience and intensity of stimuli has been a topic of considerable debate<sup>13</sup>. Some evidence suggests that KCs may function as *all-or-none* responses, showing no modulation based on stimulus salience or intensity. For example, a recent study found that although unfamiliar voices initially seemed to evoke larger KCs compared to familiar voices, this difference vanished when intertrial variability in KC latency was considered<sup>18</sup>. However, this study employed strict criteria for identifying potential KCs and did not account for possible topographic variations in KC expression. In our findings, the peak-to-peak amplitude of evoked KCs was significantly larger for both negative and positive stimuli compared to neutral stimuli, with no significant amplitude differences between negative and positive stimuli. This result aligns with our observation of a stronger GFP response to negative and positive stimuli relative to neutral ones during wakefulness. Overall, these findings indicate that emotional stimuli, whether

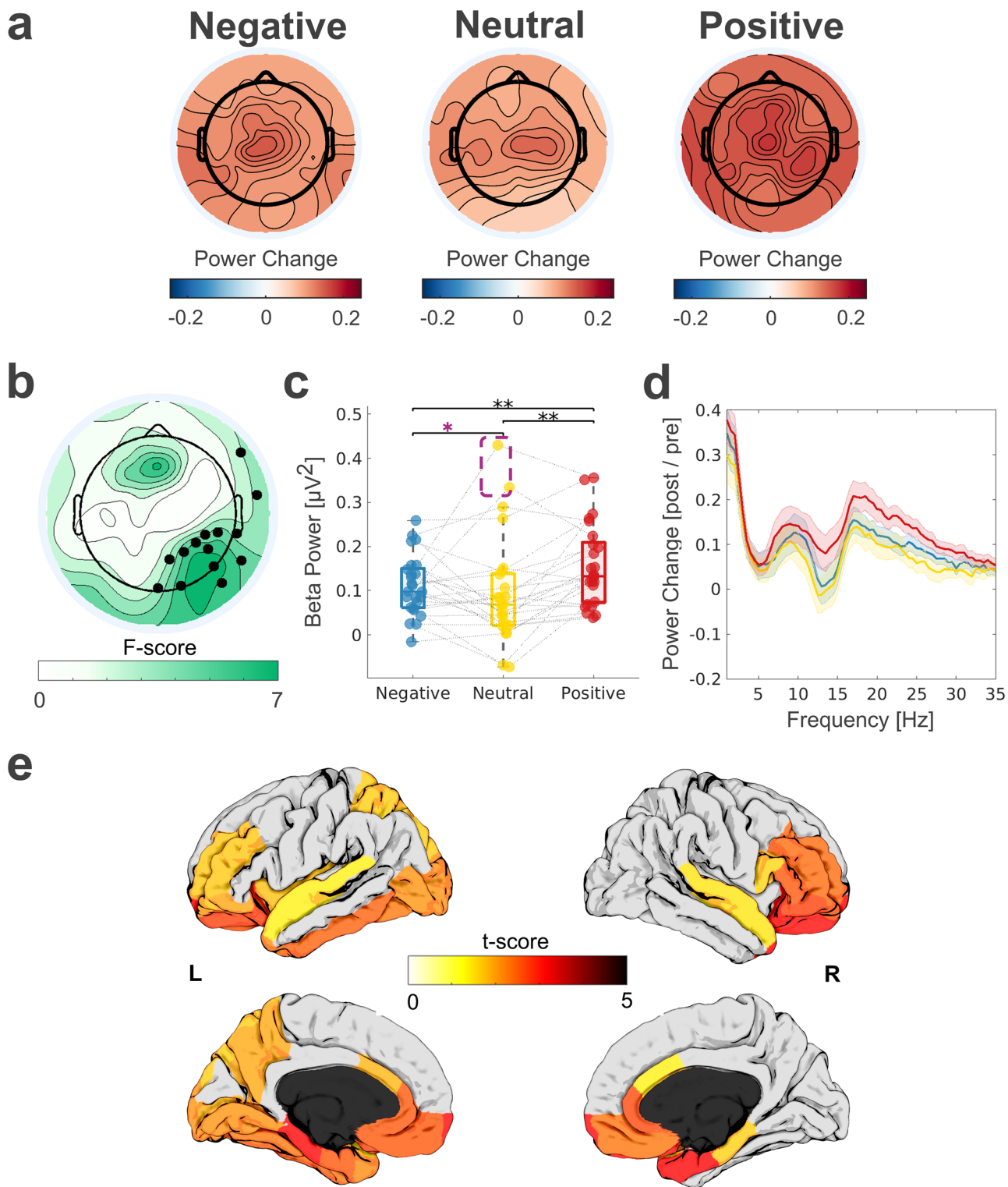


**Fig. 8 | Changes in signal power after evoked KCs.** **a** Topographic distribution of relative beta-power changes (18–30 Hz) for the three valence classes. **b** Results of the topographic rmANOVA for beta power variations across valence classes. Black dots mark electrodes showing a significant effect with  $p < 0.05$ , cluster-mass correction. **c** Post-hoc comparisons between valence classes. Each dot represents average values computed within the cluster of electrodes shown in **b** for each subject. The purple dashed line marks two outliers in the neutral condition. After removal of these

outliers the contrast between negative and neutral stimuli becomes significant (purple \*).  $*p < 0.05$ ,  $**p < 0.01$ ,  $***p < 0.001$ . **d** Mean spectral power changes after KCs computed as  $\log(\text{power}_{\text{post}}) - \log(\text{power}_{\text{pre}})$  for each valence class (mean across electrodes depicted in **b**). **e** Source modeling analysis showing significant beta-power change differences between positive and neutral stimuli ( $q < 0.05$ , FDR correction). Medial structures depicted in black were not modeled and tested. Box-plots whiskers represent  $\pm 1.5$  IQR from Q1/Q3.

positive or negative, tend to elicit more robust neural responses during both wakefulness and sleep.

Further analyses assessing the topographic distribution of the different components of evoked KCs revealed that negative-valence stimuli were associated with a stronger negative EEG component (N550) across most central, frontal, and lateral electrodes relative to neutral stimuli. The late positive component of the KCs (P900) was instead stronger for both positive and negative stimuli relative to neutral ones in centro-temporal and frontal electrodes. Consistent with this, we also found that the time-window between N550 and P900 was associated with stronger increases in alpha/sigma and beta power for affectively-charged stimuli relative to neutral ones. On the other hand, no significant differences were found for the early positive KC component (P200). Moreover, no significant differences were found between positive and negative stimuli for any of the examined KC components. Overall, these results indicate that late KC components (N550-P900) may be more sensitive to affective information potentially relevant for the sleeper than the early P200 component. This observation is consistent with evidence suggesting that the early and late components of the KC may reflect different functional processes<sup>14,15</sup>.

Notably, both scalp and source modeling analyses revealed that the strongest differences in N550 and P900 amplitudes occurred in centro-temporal and centro-frontal areas, roughly corresponding to somatomotor and auditory cortices. This topographical distribution is consistent with previous evidence indicating that KC responses integrate both a modality-nonspecific component—likely driven by arousal-related structures with preferential projections to somatomotor areas—and a sensory modality-specific response involving primary sensory cortices<sup>36</sup>. Our results suggest that both of these systems may be modulated by the emotional salience of external stimuli.

### Stimulus valence influences post-KC brain activity changes

Previous work showed that KCs and KC-like slow waves (collectively indicated as *type I* waves) are followed by relative changes in brain activity that may persist for a few seconds, including increases in delta, alpha, and beta activity, and a decrease in sigma activity reflecting a temporary suppression of thalamocortical spindles (11–15 Hz)<sup>11,16,37</sup>. Recent work showed that KCs induced by unfamiliar voices are associated with stronger increases in beta activity relative to KC triggered by familiar voices<sup>18</sup>. The authors suggested that such an increased beta activity may reflect a promoting effect of KCs on the processing of subsequent relevant sensory information during NREM sleep. In line with this view, Legendre and colleagues showed that the few seconds after a KC are associated with an amplification in the processing of relevant (vs. non-relevant) external signals<sup>17</sup>. Consistent with these observations, here we found that KCs evoked by negative and positive stimuli, relative to those induced by neutral stimuli, are followed by stronger increases in beta activity in the few seconds after the KC itself, especially in temporo-parietal and prefrontal areas. This spatial pattern appears to largely overlap with brain functional systems involved in affective processing<sup>38</sup>. Interestingly, the observed effects were stronger for positive than for negative stimuli. Taken in the context of the other results described in this work, it appears that while both negative and positive stimuli induce stronger KC-related responses relative to neutral stimuli, the effects of the two valence classes may partially differ over time, with late responses being stronger for positive than negative stimuli. This “amplification” of arousal-like activity for positive stimuli is consistent with evidence indicating a relative attentional bias for positive relative to negative stimuli during wakefulness<sup>20,21,39,40</sup>. Of note, though, previous research suggests that this bias may be more evident in the early stages of stimulus processing. The difference observed here could reflect a slower and/or partially different processing of affective stimuli during sleep relative to wakefulness.

### The KC as part of a longer multi-phasic stimulus-related response

Evoked KCs are classically regarded as “*Janus-faced*” events due to their combination of slow-wave-like appearance and reactive nature<sup>8</sup>. Moreover,

KCs are usually defined as *all-or-none*, stereotypical events<sup>41,42</sup>. Our present findings indicate that KCs should be regarded as the initial part of a multi-phasic stimulus-related brain response unfolding over several seconds, whose different components show different levels of stimulus-dependent modulation. Previous work suggested that early components of the KC may reflect the activation of both sensory-specific and non-sensory-specific, arousal-related pathways<sup>14,36,42</sup>. Indeed, activation patterns induced by different sensory modalities show both overlapping fronto-central components and distinct sensory-specific responses. Here, we found that auditory evoked KCs begin to differ according to the valence of stimuli starting from the main negative wave component. The wave negative-to-positive transition is characterized by the appearance of spindle-like activity and increases in beta power<sup>10,11,16,18,37</sup>. All these elements are modulated by stimulus valence, with stronger activity changes for negative and positive relative to neutral stimuli. Then, KCs and KC-like slow waves are followed by arousal-like brain activity changes, including increases in delta, alpha, and beta activity, in combination with a temporary suppression of spindling activity<sup>11,16,37</sup>. This late phase, evident 2–6 s after the KC, may correspond to a *sentinel mode* period<sup>18,19</sup>, in which novel relevant stimuli may receive enhanced processing and more easily induce an awakening<sup>7,17</sup>. Interestingly, this *sentinel state* following evoked KCs appears to be modulated as a function of the affective saliency of the incoming stimulus<sup>17–19,26</sup>.

These observations suggest that the KC may act as an initial “quenching” mechanism for stimulus processing at the cortical level, with more salient and arousing stimuli evoking larger (i.e., more synchronous) neural responses. However, this initial suppression is incomplete, as post-KC activity continues to carry information about the stimulus’s (affective) salience. In this context, stronger increases in wake-like activity may indicate a state of heightened awareness of the external environment during sleep, enhancing the detection of and response to subsequent relevant stimuli.

### Spontaneous slow waves block the processing of sensory information

Spontaneous slow waves, reflecting the alternation of neuronal activation and silence, have been previously suggested to have a key role in reducing the level of consciousness and ensuring sensory disconnection during sleep<sup>43,44</sup>. Indeed, the occurrence of local slow waves out of phase across distinct regions may limit the ability of different cortical areas to effectively communicate among each other<sup>45–47</sup>. Moreover, sensory information reaching neurons during an off-state may not undergo further processing as those neurons might be unable to properly respond to the stimulation (e.g.,<sup>48</sup>). Indeed, research in rats indicates that higher amplitudes of spontaneous slow waves and shorter latencies before stimulus presentation are associated with a decreased occurrence of evoked slow waves<sup>49</sup>. Consistent with this, here we found that, of those stimuli that did not trigger a KC (i.e., ~15% of all stimuli), about 60% occurred during a spontaneous slow wave. Interestingly, we also noted that while some spontaneous slow waves did not prevent the appearance of a KC, those that did so were associated with a stronger involvement of bilateral central and parietal electrodes. Overall, these findings indicate that the activation of the arousal system by external stimuli is not sufficient, per-se, to trigger a KC, whose appearance also depends on the state of cortical neurons. Moreover, they suggest that while spontaneous slow waves may contribute to reducing the processing of sensory information, such a reduction may be less efficient during the so-called “*light sleep*” (N1/N2), when slow waves are sparse and small. In this phase of sleep, evoked KCs may have a more crucial role in attenuating or suppressing incoming information. However, due to the limited number of trials without evoked KCs in our study, these findings warrant further investigation. Future research should include larger sample sizes and specifically examine the influence of other oscillatory patterns, such as sleep spindles, as well as spontaneous fluctuations in ongoing brain activity on the brain’s response to emotionally charged stimuli.

### Conclusions

In summary, our study demonstrates that the KC is not an *all-or-none* phenomenon and that this wave is part of a longer, multi-phasic response

whose elements may be distinctively modulated by stimulus (affective) salience. Indeed, our results indicate that the likelihood of KC generation, the morphology and topographic distribution of the KC, as well as early and late post-KC brain activity changes, are all modulated by stimulus affective valence. This multiphasic response and its flexibility may contribute to guarantee an optimal balance between the needs for sleep continuity and prompt reactivity to possible dangers or opportunities in physiological conditions.

## Material and methods

### Participants

Thirty-three healthy adults (age:  $27.15 \pm 2.98$  years, 18 females) were recruited through word of mouth and participated in the study. A preliminary screening interview was conducted to assess eligibility based on inclusion and exclusion criteria. Volunteers were included if they reported 6–9 h of sleep per night and good subjective sleep quality, with no self-reported history or presence of neurological, psychiatric, or sleep disorders. We excluded volunteers who were taking medications known to significantly affect brain function and sleep. Women who were pregnant or breastfeeding at the time of the study were also excluded.

The study was approved by the local Ethical Committee (Comitato Etico di Area Vasta Nord Ovest Regione Toscana, protocol n. 24579/2018). Each participant signed a written informed consent before taking part in the experiment. All ethical regulations relevant to human research participants were followed. The experimental protocol adhered to the principles of the Declaration of Helsinki (2013).

Eight volunteers were excluded because they failed to reach or maintain stable NREM sleep during the stimulation protocol. Therefore, the final sample included a total of 25 participants (age:  $27.6 \pm 2.8$  years, range 22–32 years; 12 females).

### Stimuli

Stimuli consisted of non-verbal utterances commonly referred to as vocal bursts. A total of 192 vocal bursts, including an equal number of negative, neutral, and positive valence stimuli, were obtained from a previously published dataset<sup>29,50</sup>. Specifically, the initial pool of stimuli included 2032 vocal bursts recorded from 56 speakers (26 F, age range 18–35 years) and representing a wide range of emotional states. Since vocal bursts in this pool had very different durations, the stimuli were modified (stretched or compressed) to obtain a duration of exactly 850 ms. To avoid excessive distortions, stimuli that would have had to be stretched or compressed in time by more than 50% of their original duration (i.e., shorter than 567 ms or longer than 1700 ms) were discarded at this stage. We retained a total of 1008 vocal bursts. The stretching/compression procedure was performed using a pitch-preserving algorithm (audioStretch, phase-vocoder method), which allowed us to preserve the spectral properties of the stimuli (e.g., fundamental frequency, speech harmonics). Finally, stimuli were normalized in loudness according to the EBU R 128 Standard.

As detailed elsewhere<sup>33</sup>, twelve volunteers (age:  $29.0 \pm 2.1$  years; 6 females) listened and rated the valence and arousal levels of all stimuli using 0–100 scales. Raters were instructed to focus on the speaker's affective state. We normalized the raw arousal and valence scores using the z-score transformation for each rater and computed the average across raters. Then, we discarded stimuli associated with low arousal scores (z-score < 0). The retained stimuli were further classified based on their valence as follows: negative = z-score < -1; neutral within  $\pm 0.5$  z-score range; positive = z-score > +1. These criteria led to the selection of 267 stimuli. To ensure an equal number of stimuli across valence classes, we identified the valence class containing the smallest number of stimuli and selected an identical number of stimuli in the other two classes. This led to the selection of 64 stimuli per class (Fig. 1a and Supplementary Fig. 7). For neutral stimuli, we selected the 64 vocal bursts that showed the lowest standard deviation in valence scores across raters. This approach was used to avoid including stimuli that exhibit neutral average scores but show relatively inconsistent valence ratings across participants<sup>33</sup>. For negative stimuli, we generated 1000

random selections of 64 stimuli and randomly chose one set of negative stimuli showing no arousal difference with respect to positive stimuli ( $p = 0.998$ ). It should be noted that while negative and positive stimuli did not differ in arousal scores, significant differences were found between these valence classes and neutral stimuli ( $p < 0.001$ ), in line with the commonly observed v-shaped distribution of valence-arousal scores in affective ratings (Fig. 1a)<sup>33,51–54</sup>.

### Protocol and procedures

Each participant completed first a sleep (overnight) and then a wakefulness experimental session (Fig. 1b). Both sessions combined a continuous high-density (hd)-EEG recording (64 channels, 500 Hz sampling rate; Magstim-EGI) and an auditory stimulation protocol involving the presentation of vocal bursts with negative, neutral, and positive affective valence. The wakefulness EEG recordings were followed by a behavioral affective rating task in which participants had to rate each vocal burst in terms of arousal and valence (see below). During both the wakefulness and sleep sessions, stimuli were delivered through in-ear headphones (RHA model: MA750), with presentation controlled via custom scripts developed using *Psychtoolbox* (v3.0.17<sup>55</sup>) and MATLAB<sup>56</sup>, version 2019b). The order of the stimuli was randomized for each experimental session and participant. The two experimental sessions, always performed in the same order, were spaced one to four weeks. All experimental procedures were performed in a sound-attenuated chamber (BOXY, B-Beng s.r.l., Italy).

The overnight session was scheduled according to the participants' usual bedtime. Auditory stimulation was manually started after ~15 min of stable N2 sleep. At the beginning of the procedure, "probe" vocal bursts distinct from those employed as experimental stimuli were presented and used to determine an optimal, individualized stimulation volume. Specifically, the volume was adjusted based on the participant's response: decreased if the stimuli induced major arousals or awakenings, or increased if they failed to elicit a KC-like response. Once an optimal volume was established (typically around 35 dB), it was kept constant throughout the entire stimulation session. The experimenters initiated the presentation of the actual experimental stimuli and continuously monitored the EEG recording. Specifically, they paused the stimulation in the case of arousals, awakenings, or transitions to REM sleep, resuming it once stable N2 sleep was reached again. Auditory stimulation was administered only during the first part of the night, after which the EEG cap was removed, and participants were allowed to complete their sleep undisturbed to minimize discomfort and maximize compliance with the study procedures. Our priority was to complete one full stimulation cycle, including a total of 192 stimuli. Each stimulus was presented only once, and the inter-stimulus interval (ISI) was randomly selected in the range between 8 and 12 s<sup>57</sup>. This ISI range was chosen based on pilot studies, which indicated that intervals longer than 8 s maximized KC probability while minimizing arousal likelihood and optimizing the overall duration of the experimental procedure.

The wakefulness session took place during daytime hours. Participants were seated comfortably in a chair with their eyes closed. As for the sleep session, each stimulus was presented only once. The ISI was randomly selected in the range between 3 and 7 s. A standard volume of ~50 dB was used. After the presentation of all stimuli, participants were offered a 10-min break and subsequently completed an affective rating task in which they had to provide valence and arousal scores for each stimulus. Specifically, stimuli were again presented one by one at the same volume used during the night experimental session, and participants expressed their ratings for each stimulus using two 0–100 visual-analog scales (VAS) presented through a custom MATLAB graphical user interface.

### Sleep scoring

Offline sleep scoring was performed over 30-s epochs following standard criteria by an expert operator blinded to the stimulation procedure (see Supplementary Figs. 8 and 9). Four of the electrodes near the eyes were used to monitor eye movements, while electrodes overlying the masseter muscles and close to the chin were used to monitor muscle tone<sup>58</sup>.

## Sleep EEG data preprocessing

All recordings were preprocessed using a custom, automated pipeline based on the combination of different plugins and functions available in the EEGLAB toolbox<sup>59</sup>. First, a copy of the raw data was created and filtered between 0.5 and 40 Hz (*pop\_eegfiltnew* function; high-pass filter at 0.5 Hz, stopband 0.25 Hz; low-pass filter at 40 Hz, stopband 45 Hz; notch filter between 47 and 53 Hz, stopband 48–52 Hz; window type: *Hamming*). Then, potential electrical bridges were identified using the *eBridge* tool<sup>60</sup>. Moreover, bad channels were identified using the *findNoisyChannels* function available within the *PREP-pipeline* plugin<sup>61</sup>. The detected bridged and bad channels were excluded from both the raw (unfiltered) and filtered data. Then, EEG artifacts were reduced using a procedure based on *independent component analysis* (ICA). Since ICA assumes data stationarity, we applied preprocessing steps to mitigate violation of this assumption, including filtering and segment rejection of rare non-stereotypical events<sup>62</sup>. Additionally, we restricted ICA to N2/N3 epochs to maximize homogeneity in neural and artifactual sources. Specifically, the filtered copy of the raw data was divided into non-overlapping 1-s segments. Then, the EEGLAB *pop\_jointprob* function was used to identify and reject segments containing major artifacts (local threshold and global threshold were set to 3 SDs). All segments that did not belong to NREM epochs were also discarded. The analysis was performed using the *runica* EEGLAB function. The *ICLabel* plugin<sup>63</sup> was used to classify the obtained ICs as representing brain or artifactual activity. We rejected all the ICs with a “brain” classification probability lower than 25%. Among the remaining ICs, we retained those that were classified as “brain” activity and those identified as “non-brain,” for which “brain” represented the second highest probability. On average, we removed  $67.58 \pm 8.96\%$  of identified ICs (range: 48.33%–82.25%) in sleep data and  $56.00 \pm 9.24\%$  of identified ICs (range: 34.78%–71.43%) in wakefulness data. The removed components included single-channel artifacts, residual eye movements, cardiac activity, and sweating-related artifacts (Supplementary Fig. 10). The ICA weights obtained from this procedure and the indices of the ICs to be retained were eventually applied to the raw, unfiltered, continuous recording. Finally, the signals of rejected channels were interpolated from nearby channels using spherical splines (EEGLAB *pop\_interp* function).

In order to identify and reject stimulation trials associated with residual artifactual activity, the preprocessed signal was filtered between 0.5 and 40 Hz, and segmented into epochs of 5.5 s, from  $-2$  to  $+3.5$  s with respect to stimulus onset. Bad stimulation trials identified using the *pop\_jointprob* function were excluded from all subsequent analyses. Overall, we rejected  $11.28 \pm 5.00\%$  of all trials (no differences between valence classes; rmANOVA,  $F(2,48) = 0.41$ ,  $p = 0.66$ ).

## Slow-wave detection and analysis

For each stimulation trial, we defined as an evoked KC the largest slow-wave-like response (if any) peaking between 0.25 and 1.75 s after stimulus onset. This time window was chosen by taking into account the fact that KCs have a peak frequency around or below 1 Hz, meaning their full waveform (negative peak followed by a positive rebound) unfolds over  $\sim 1$ –2 s. The selected bounds allowed us to exclude early responses unlikely to reflect stimulus-evoked KCs while ensuring that delayed but plausibly stimulus-related KCs were still considered. Slow waves were detected automatically in a composite EEG signal generated from filtered (0.5–40 Hz) and linked-mastoid-referenced channels, as described in previous work<sup>12,64</sup>. This method provides a single time reference (across electrodes) for each slow wave and facilitates the detection of both local and widespread events. Specifically, a negative-going signal envelope was calculated by averaging, for each time-point, the three most negative samples (electrodes) after discarding the single most negative value. This approach was used to minimize the potential impact of any residual large-amplitude artifactual activity in isolated electrodes. The resulting signal was band-pass filtered between 0.5 and 4 Hz (Chebyshev type II filter) before the application of a slow-wave detection procedure based on half-wave zero-crossings<sup>12,34</sup>. Only negative half-waves with a duration of between 0.25 and 1.25 s ( $< 2$  Hz) were

retained for further analyses. No amplitude thresholds were applied to avoid making strong a priori assumptions about possible stimulus-dependent variations in the amplitude of evoked slow waves. Instead, we considered any slow wave occurring within the predefined time window as a potential stimulus-evoked KC. Of note, though, the applied slow-wave detection method intrinsically excludes small amplitude fluctuations, ensuring that low-voltage noise does not influence the analysis. If multiple slow waves were detected within the time window of interest, only the largest event was selected. However, additional analyses examining the presence of sequential slow-wave events (slow-wave trains) and their relationship to stimulus valence are presented in Supplementary Figs. 11 and 12.

Since the negative-envelope signal does not allow for the identification of meaningful positive signal deflections around the negative half-wave, we determined for each detected wave the actual EEG channel that recorded the largest negative peak (i.e., the prototypical wave<sup>65</sup>). For this, we applied the same slow-wave detection approach described above to the signal of each electrode and limited our search to a time window of 40 ms centered around the peaks of slow waves detected using the negative-envelope method. For all the prototypical slow waves, various parameters of interest were calculated and stored, including the timing of the negative peak, the timing of the largest positive peaks preceding and following the negative half-wave, and the amplitude (in  $\mu$ V) of such peaks. For evoked KCs, the early and late positive peaks are commonly referred to as P200 and P900, respectively<sup>13</sup>. We defined slow-wave peak-to-peak amplitude as the absolute voltage difference between the maximum wave negative peak (also indicated as N550) and the maximum subsequent positive peak (P900). Moreover, we defined the scalp “involvement” for each wave and peak of interest as the mean EEG signal calculated for all electrodes in a 40 ms window centered on the wave peaks.

## Time-frequency analysis

A KC-locked time-frequency analysis was performed to investigate possible effects of stimulus affective valence on high-frequency signal components. Time-frequency decomposition was performed using the *FieldTrip* toolbox for each stimulation trial and channel, from unfiltered data. This analysis covered the 2–42 Hz frequency range (in steps of 2 Hz), and spanned the time window between  $-2$  and 3.5 s relative to stimulus onset (in steps of 0.02 s). The signal power at each frequency of interest and time point was estimated using complex Morlet wavelets<sup>66,67</sup>. The length of the wavelets increased linearly from 4 to 10 cycles as frequency increased (21 frequency steps), allowing for a balance between temporal precision at lower frequencies and frequency resolution at higher frequencies. Then, the average across trials was computed at the individual level for negative, neutral, and positive stimuli. A baseline correction was applied for each trial and then again on the average across trials, using the mean activity extracted from the time window between  $-0.7$  and  $-0.3$  s relative to stimulus onset. The baseline was kept temporally distant from the stimulus onset to avoid the leakage of post-stimulus activity into the baseline period<sup>68</sup>. Noisy epochs for each participant within each condition were then rejected based on the joint probability across channels (*pop\_jointprob* function<sup>69</sup>; rmANOVA for rejected epochs across valence classes,  $p = 0.143$ ). Trials in which a KC was not identified were also excluded (see Results). To assess statistical differences between valence classes, the activity time-locked to evoked KCs was extracted between  $-0.25$  and  $+1.25$  s relative to the KC maximum negative peak in each trial. The analyses focused on the 2–30 Hz frequency range.

## Power analysis

Previous work showed that KCs are followed by relative changes in brain activity that last for a few seconds<sup>11,16,37</sup>. In particular, increases in signal power are observed in the delta, alpha, and beta ranges, potentially indicating the coexistence of arousal-like responses and increased slow-wave activity (e.g., delta bursts). Therefore, here we explored whether such post-KC variations differed between negative, neutral, and positive stimuli. For each trial, the signal power spectral density (PSD) was estimated for each electrode in the 2 s before the stimulation (*pre*) and in two non-overlapping

2-s windows starting 2 s after the maximum negative peak of the evoked KC (*post*). In each window, PSD was computed using the multitapers method with a fixed spectral smoothing of  $\pm 1$  Hz. Then, we computed the signal power in the delta (1–4 Hz), alpha (8–12 Hz), and beta (18–30 Hz) frequency ranges. The signal power obtained in the post-KC windows was averaged to obtain a single value per trial. Then, we calculated the post-KC power variation using the formula:  $\log(\text{power\_post}) - \log(\text{power\_pre})$ .

### Source modeling analysis

Differences detected by topographic comparisons were further explored through source modeling to obtain a more accurate characterization of regional brain activity variations as a function of stimulus valence. To perform signal source estimation, we used the *MNE-Python* software (version 1.5.0;<sup>70</sup>). The source reconstruction was computed for all trials that included a KC response, in a 1-s window centered on the maximum wave negative peak (N550). The “*fsaverage*” template was used to define the boundary element model (BEM). This template is based on a combination of 40 brain MRI scans and is available within the *FreeSurfer* software.<sup>71</sup>. Starting from this head model, we generated a 3-layer BEM (outer-skin, outer-skull, inner-skull; respective conductivity: 0.3, 0.006, 0.3), and coregistered it to the sensor space defined according to a predefined set of standard electrode positions. The surface source space was represented using 8196 vertices across the two hemispheres. We used the dynamic statistical parametric maps (dSPM) algorithm<sup>72</sup> and a regularized covariance matrix computed from the whole time series of the epochs to obtain the inverse solution. Moreover, we assigned a constrained loose orientation of 0.2 to sources, and applied a depth whitening value of 4. Finally, we computed the root sum square of the three reconstructed dipole orientations, obtaining a single source time series for each vertex. Given the inherent limitations in spatial accuracy associated with using standardized head models and template electrode positions, we adopted an atlas-based approach focusing on relatively large cortical regions. This strategy mitigates the impact of potential localization errors, which have been reported to reach up to 2 cm when using generic head models compared to anatomically accurate individual-specific models.<sup>73</sup>. Specifically, we parceled the brain surface according to the Desikan-Killiany Atlas<sup>74</sup> and averaged signal values within each parcel to obtain the respective regional brain activity estimate. To assess significant regional differences across conditions, we computed the mean signal in a 40 ms time window centered on the KC negative peak. An identical procedure was used to compute the sources of the P900 component of the KC. Moreover, for frequency bands showing significant valence-related differences in pre-to-post KC power changes at scalp level, the analyses were repeated at source level.

### Waking EEG and behavioral data preprocessing

Affective ratings collected during the wakefulness session were analyzed to validate the classification of stimulus valence into negative, neutral, and positive categories (see Stimuli section). Specifically, we evaluated the consistency of the original study’s ratings with those obtained in the current study by comparing average valence and arousal scores using Spearman’s rank correlation and linear regression.

EEG data preprocessing was performed using the same automated pipeline applied to sleep recordings. In this case, a different low-pass filter was applied to allow preserving frequencies up to 45 Hz (stopband: 50.62 Hz; transition band width: 11.25 Hz). In order to identify and reject stimulation trials associated with residual artifact activity, the pre-processed signal was filtered and segmented into 4.5-s epochs, from  $-1.5$  to  $+3$  s relative to stimulus onset. Then, the signal of each trial was baseline corrected using a 1-s pre-stimulus window. Bad stimulation trials identified using the *pop\_jointprob* function were excluded from all subsequent analyses ( $12.29 \pm 4.56\%$  of all trials were rejected on average; no differences between valence classes; rmANOVA,  $F(2,48) = 0.05$ ,  $p = 0.95$ ). To identify potential differences in stimulus-evoked responses across valence classes we computed the *global field potential* (GFP), which is a measure of the strength of the scalp potential field. The GFP is calculated as the standard deviation of

electrode voltages at a given time point<sup>75</sup>. An important advantage of this index relative to standard event-related potential analyses is that it does not involve any a priori assumptions regarding where (in which electrodes) scalp EEG changes should be expected to occur or differ across conditions.

### Statistics and reproducibility

The properties of slow waves associated with stimulus presentation (probability of occurrence, amplitude, latency) and GFP changes in wakefulness were compared across valence classes using repeated-measure (rm)ANOVAs. Post-hoc comparisons were performed using paired *t*-tests. For topographic analyses, corrections for multiple comparisons were applied using permutation-based cluster-mass corrections<sup>76</sup>. In brief, each test was repeated ( $N = 1000$ ) after shuffling the labels of the valence classes, and all clusters of significant electrodes were identified ( $p < 0.05$ ). Then, we computed the sum of test statistics across electrodes belonging to the same cluster, and the maximum obtained value was saved in a frequency table. A minimum cluster-mass threshold corresponding to the 95th percentile of the resulting distribution was applied to correct for multiple comparisons<sup>77</sup>. A similar approach was used for GFP-based analyses, although in this case, clusters were formed over time points, rather than across electrodes.

For time-frequency decompositions, comparisons between valence classes (negative vs. neutral, positive vs. neutral, and negative vs. positive) were performed with a cluster-based permutation using *t*-tests for dependent samples.<sup>78</sup> Of note, the same contrasts were performed for each electrode, for each time-point in a time-window from  $-250$  ms to  $+1250$  ms relative to the KC negative peak, and in the frequency range between 2 Hz and 30 Hz. Corrections for multiple comparisons were applied using a non-parametric, Monte Carlo-based statistical approach with 5000 permutations. Cluster-level statistics were calculated taking the sum of the *t*-values within every cluster (minimum neighbor channels = 2; alpha level = 0.05, two-tailed, accounting for both positive and negative clusters).

For analyses in source space, an FDR correction was applied to account for multiple comparisons across tested cortical brain regions.

### Reporting summary

Further information on research design is available in the Nature Portfolio Reporting Summary linked to this article.

### Data availability

The source data underlying the graphs and charts presented in this study are provided in the Supplementary Data. Raw data and additional supporting materials are available from the corresponding author upon reasonable request.

Received: 4 November 2024; Accepted: 3 July 2025;

Published online: 17 July 2025

### References

1. Anafi, R. C., Kayser, M. S. & Raizen, D. M. Exploring phylogeny to find the function of sleep. *Nat. Rev. Neurosci.* **20**, 2 (2019). Article.
2. Sotelo, M. I., Tyan, J., Dzera, J. & Eban-Rothschild, A. Sleep and motivated behaviors, from physiology to pathology. *Curr. Opin. Physiology* **15**, 159–166 (2020).
3. Simon, K. C., Nadel, L. & Payne, J. D. The functions of sleep: a cognitive neuroscience perspective. *Proc. Natl. Acad. Sci. USA* **119**, e2201795119 (2022).
4. Bonnet, M. H. & Arand, D. L. Clinical effects of sleep fragmentation versus sleep deprivation. *Sleep. Med. Rev.* **7**, 297–310 (2003).
5. Boon, M. E., van Hooff, M. L. M., Vink, J. M. & Geurts, S. A. E. The effect of fragmented sleep on emotion regulation ability and usage. *Cognit. Emot.* **37**, 1132–1143 (2023).
6. Joiner, W. J. Neuroscience: sleep fragmentation impairs memory formation. *Curr. Biol.* **29**, R1181–R1184 (2019).
7. Andrlon, T. & Kouider, S. The vigilant sleeper: neural mechanisms of sensory (de)coupling during sleep. *Curr. Opin. Physiol.* **15**, 47–59 (2020).

8. Halász, P. K-complex, a reactive EEG graphoelement of NREM sleep: an old chap in a new garment. *Sleep. Med. Rev.* **9**, 391–412 (2005).
9. De Gennaro, L., Ferrara, M. & Bertini, M. The spontaneous K-complex during stage 2 sleep: is it the ‘forerunner’ of delta waves?. *Neurosci. Lett.* **291**, 41–43 (2000).
10. Cash, S. S. et al. The human K-complex represents an isolated cortical down-state. *Science* **324**, 1084–1087 (2009).
11. Bernardi, G., Siclari, F., Handjras, G., Riedner, B. A., & Tononi, G. Local and widespread slow waves in stable NREM sleep: evidence for distinct regulation mechanisms. *Front. Hum. Neurosci.* **12**, <https://www.frontiersin.org/articles/10.3389/fnhum.2018.00248> (2018).
12. Siclari, F. et al. Two distinct synchronization processes in the transition to sleep: a high-density electroencephalographic study. *Sleep* **37**, 1621–1637 (2014).
13. Colrain, I. M. The K-complex: a 7-decade history. *Sleep* **28**, 255–273 (2005).
14. Laurino, M. et al. Disentangling different functional roles of evoked K-complex components: mapping the sleeping brain while quenching sensory processing. *NeuroImage* **86**, 433–445 (2014).
15. Laurino, M., Piarulli, A., Menicucci, D., & Gemignani, A. Local gamma activity during non-REM sleep in the context of sensory evoked K-complexes. *Front. Neurosci.* **13**, <https://www.frontiersin.org/articles/10.3389/fnins.2019.01094> (2019).
16. Halász, P. Arousals without awakening—dynamic aspect of sleep. *Physiol. Behav.* **54**, 795–802 (1993).
17. Legendre, G., Andrillon, T., Koroma, M. & Kouider, S. Sleepers track informative speech in a multitalker environment. *Nat. Hum. Behav.* **3**, 274–283 (2019).
18. Ameen, M. S., Heib, D. P. J., Blume, C. & Schabus, M. The brain selectively tunes to unfamiliar voices during sleep. *J. Neurosci.* **42**, 1791–1803 (2022).
19. Blume, C., del Giudice, R., Wislowska, M., Heib, D. P. J. & Schabus, M. Standing sentinel during human sleep: continued evaluation of environmental stimuli in the absence of consciousness. *NeuroImage* **178**, 638–648 (2018).
20. Fredrickson, B. L. & Branigan, C. Positive emotions broaden the scope of attention and thought-action repertoires. *Cognit. Emot.* **19**, 313–332 (2005).
21. Pool, E., Brosch, T., Delplanque, S. & Sander, D. Attentional bias for positive emotional stimuli: a meta-analytic investigation. *Psychol. Bull.* **142**, 79 (2016).
22. Beh, H. C. & Barratt, P. E. H. Discrimination and conditioning during sleep as indicated by the electroencephalogram. *Science* **147**, 1470–1471 (1965).
23. Perrin, F., García-Larrea, L., Mauguière, F. & Bastuji, H. A differential brain response to the subject’s own name persists during sleep. *Clin. Neurophysiol.* **110**, 2153–2164 (1999).
24. Blume, C. et al. Preferential processing of emotionally and self-relevant stimuli persists in unconscious N2 sleep. *Brain Lang.* **167**, 72–82 (2017).
25. Chen, C., Sung, J.-Y., & Cheng, Y. Neural dynamics of emotional salience processing in response to voices during the stages of sleep. *Front. Behav. Neurosci.* **10**, <https://www.frontiersin.org/articles/10.3389/fnbeh.2016.00117> (2016).
26. Moyne, M. et al. Brain reactivity to emotion persists in NREM sleep and is associated with individual dream recall. *Cereb. Cortex Commun.* **3**, <https://doi.org/10.1093/texcom/tgac003> (2022).
27. van Sweden, B., van Dijk, J. G. & Caekebeke, J. F. V. Auditory information processing in sleep: habituation to repetitive stimuli. *Neuropsychobiology* **30**, 143–147 (1994).
28. Brooks, J. A. et al. Deep learning reveals what vocal bursts express in different cultures. *Nat. Hum. Behav.* **7**, 2 (2023). Article.
29. Cowen, A. S., Elfenbein, H. A., Laukka, P. & Keltnner, D. Mapping 24 emotions conveyed by brief human vocalization. *Am. Psychol.* **74**, 698–712 (2019).
30. Pell, M. D. et al. Preferential decoding of emotion from human non-linguistic vocalizations versus speech prosody. *Biol. Psychol.* **111**, 14–25 (2015).
31. Sauter, D. A., Eisner, F., Ekman, P. & Scott, S. K. Cross-cultural recognition of basic emotions through nonverbal emotional vocalizations. *Proc. Natl. Acad. Sci. USA* **107**, 2408–2412 (2010).
32. Sauter, D. A., Eisner, F., Ekman, P. & Scott, S. K. Emotional vocalizations are recognized across cultures regardless of the valence of distractors. *Psychol. Sci.* **26**, 354–356 (2015).
33. Grollero, D. et al. The structure underlying core affect and perceived affective qualities of human vocal bursts. *Cognit. Emot.* **37**, 1–17 (2023).
34. Riedner, B. A. et al. Sleep homeostasis and cortical synchronization: III. A high-density EEG study of sleep slow waves in humans. *Sleep* **30**, 1643–1657 (2007).
35. Lechat, B. et al. K-complexes are a sensitive marker of noise-related sensory processing during sleep: a pilot study. *Sleep* **44**, <https://doi.org/10.1093/sleep/zsab065> (2021).
36. Bellesi, M., Riedner, B. A., Garcia-Molina, G. N., Cirelli, C., & Tononi, G. Enhancement of sleep slow waves: underlying mechanisms and practical consequences. *Front. Syst. Neurosci.* **8**, 208 (2014).
37. Siclari, F., Bernardi, G., Cataldi, J. & Tononi, G. Dreaming in NREM sleep: a high-density EEG study of slow waves and spindles. *J. Neurosci.* **38**, 9175–9185 (2018).
38. Lindquist, K. A., Satpute, A. B., Wager, T. D., Weber, J. & Barrett, L. F. The brain basis of positive and negative affect: evidence from a meta-analysis of the human neuroimaging literature. *Cereb. Cortex* **26**, 1910–1922 (2016).
39. Bradley, M. M. Natural selective attention: orienting and emotion. *Psychophysiology* **46**, 1–11 (2009).
40. Brosch, T., Sander, D., Pourtois, G. & Scherer, K. R. Beyond fear: rapid spatial orienting toward positive emotional stimuli. *Psychol. Sci.* **19**, 362–370 (2008).
41. Bastuji, H. & García-Larrea, L. Evoked potentials as a tool for the investigation of human sleep. *Sleep. Med. Rev.* **3**, 23–45 (1999).
42. Riedner, B. A., Hulse, B. K., Murphy, M. J., Ferrarelli, F., & Tononi, G. Temporal dynamics of cortical sources underlying spontaneous and peripherally evoked slow waves. In *Progress in Brain Research* (eds Van Someren, E. J. W. Van Der Werf, Y. D. Roelfsema, P. R. Mansvelder, H. D. & Lopes Da Silva F. H.) Vol. 193 (Elsevier, 2011).
43. Massimini, M. et al. Breakdown of cortical effective connectivity during sleep. *Science* **309**, 2228–2232 (2005).
44. Pigorini, A. et al. Bistability breaks-off deterministic responses to intracortical stimulation during non-REM sleep. *NeuroImage* **112**, 105–113 (2015).
45. Baird, B. et al. Human Rapid eye movement sleep shows local increases in low-frequency oscillations and global decreases in high-frequency oscillations compared to resting wakefulness. *eNeuro* **5**, <https://doi.org/10.1523/ENEURO.0293-18.2018> (2018).
46. Bernardi, G. et al. Regional delta waves in human rapid eye movement sleep. *J. Neurosci.* **39**, 2686–2697 (2019).
47. Funk, C. M., Honjoh, S., Rodriguez, A. V., Cirelli, C. & Tononi, G. Local slow waves in superficial layers of primary cortical areas during REM sleep. *Curr. Biol. CB* **26**, 396–403 (2016).
48. Massimini, M., Rosanova, M. & Mariotti, M. EEG slow (~1 Hz) waves are associated with nonstationarity of thalamo-cortical sensory processing in the sleeping human. *J. Neurophysiol.* **89**, 1205–1213 (2003).
49. Vyazovskiy, V. V., Faraguna, U., Cirelli, C. & Tononi, G. Triggering slow waves during NREM sleep in the rat by intracortical electrical stimulation: effects of sleep/wake history and background activity. *J. Neurophysiol.* **101**, 1921–1931 (2009).
50. Laukka, P. et al. Cross-cultural decoding of positive and negative non-linguistic emotion vocalizations. *Front. Psychol.* **4**, <https://www.frontiersin.org/articles/10.3389/fpsyg.2013.00353> (2013).

51. Kuppens, P., Tuerlinckx, F., Russell, J. A. & Barrett, L. F. The relation between valence and arousal in subjective experience. *Psychol. Bull.* **139**, 917–940 (2013).
52. Kuppens, P. et al. The relation between valence and arousal in subjective experience varies with personality and culture. *J. Personal.* **85**, 530–542 (2017).
53. Mattek, A. M., Wolford, G. L. & Whalen, P. J. A mathematical model captures the structure of subjective affect. *Perspect. Psychol. Sci.* **12**, 508–526 (2017).
54. Toet, A. et al. The relation between valence and arousal in subjective odor experience. *Chemosens. Percept.* **13**, 141–151 (2020).
55. Brainard, D. H. The psychophysics toolbox. *Spat. Vis.* **10**, 433–436 (1997).
56. The MathWorks Inc. MATLAB version: 9.7.0.1296695 (R2019b), Natick, Massachusetts: The MathWorks Inc, <https://www.mathworks.com> (2019).
57. Bastien, C. & Campbell, K. Effects of rate of tone-pip stimulation on the evoked K-Complex. *J. Sleep. Res.* **3**, 65–72 (1994).
58. Iber, C. The AASM manual for the scoring of sleep and associated events: rules, terminology, and technical specification, <https://cir.ni.ac.jp/crid/1370004237604151044> (2007).
59. Delorme, A. & Makeig, S. EEGLAB: an open source toolbox for analysis of single-trial EEG dynamics including independent component analysis. *J. Neurosci. Methods* **134**, 9–21 (2004).
60. Alschuler, D. M., Tenke, C. E., Bruder, G. E. & Kayser, J. Identifying electrode bridging from electrical distance distributions: a survey of publicly-available EEG data using a new method. *Clin. Neurophysiol.* **125**, 484–490 (2014).
61. Bigdely-Shamlo, N., Mullen, T., Kothe, C., Su, K.-M., & Robbins, K. A. The PREP pipeline: standardized preprocessing for large-scale EEG analysis. *Front. Neuroinform.* **9**, <https://www.frontiersin.org/articles/10.3389/fninf.2015.00016> (2015).
62. Stropahl, M., Bauer, A.-K. R., Debener, S., & Bleichner, M. G. Source-modeling auditory processes of EEG data using EEGLAB and brainstorm. *Front. Neurosci.* **12**, <https://www.frontiersin.org/articles/10.3389/fnins.2018.00309> (2018).
63. Pion-Tonachini, L., Kreutz-Delgado, K. & Makeig, S. ICLLabel: an automated electroencephalographic independent component classifier, dataset, and website. *NeuroImage* **198**, 181–197 (2019).
64. Mensen, A., Riedner, B. & Tononi, G. Optimizing detection and analysis of slow waves in sleep EEG. *J. Neurosci. Methods* **274**, 1–12 (2016).
65. Sousouri, G. et al. Neuromodulation by means of phase-locked auditory stimulation affects key marker of excitability and connectivity during sleep. *Sleep* **45**, <https://doi.org/10.1093/sleep/zsab204> (2022).
66. Tallon-Baudry, C. et al. Oscillatory gamma activity in humans and its role in object representation. *Trends Cogn. Sci.* **3**, 151–162 (1999).
67. Cohen, M. X. A better way to define and describe Morlet wavelets for time-frequency analysis. *NeuroImage* **199**, 81–86 (2019).
68. Cohen, M. X. *Analyzing Neural Time Series Data: Theory and Practice* (MIT Press, 2014).
69. Delorme, A., Sejnowski, T. & Makeig, S. Enhanced detection of artifacts in EEG data using higher-order statistics and independent component analysis. *NeuroImage* **34**, 1443–1449 (2007).
70. Larson, E. et al. Iuzpaz.MNE-Python (Version v1.5.0). Zenodo, <https://zenodo.org/records/8322569> (2023).
71. Fischl, B. FreeSurfer. *NeuroImage* **62**, 774–781 (2012).
72. Dale, A. M. et al. Dynamic statistical parametric mapping: combining fMRI and MEG for high-resolution imaging of cortical activity. *Neuron* **26**, 55–67 (2000).
73. Liu, C. et al. Comparison of EEG source localization using simplified and anatomically accurate head models in younger and older adults. *IEEE Trans. Neural Syst. Rehabil. Eng.* **31**, 2591–2602 (2023).
74. Desikan, R. S. et al. An automated labeling system for subdividing the human cerebral cortex on MRI scans into gyral based regions of interest. *NeuroImage* **31**, 968–980 (2006).
75. Michel, C. M. et al. Global field power: a ‘time-honoured’ index for EEG/EP map analysis. *Int. J. Psychophysiol.* **15**, 1–2 (1993).
76. Nichols, T. E. & Holmes, A. P. Nonparametric permutation tests for functional neuroimaging: a primer with examples. *Hum Brain Mapp.* **15**, 1–25 (2002).
77. Avenuti, G. et al. Emotion regulation failures are preceded by local increases in sleep-like activity. *J. Cogn. Neurosci.* **33**, 2342–2356 (2021).
78. Maris, E. & Oostenveld, R. Nonparametric statistical testing of EEG- and MEG-data. *J. Neurosci. Methods* **164**, 177–190 (2007).

## Acknowledgements

This work was in part supported by the European Union – Next Generation EU, Innovation Ecosystem “THE – Tuscany Health Ecosystem” (Mission 4, Component 2, Inv. 1.5; code ECS00000017; CUP: D63C22000400001). The authors thank Luca Cecchetti for his contributions to the development of the research protocol and the preparation of the stimuli, and Bianca Pedreschi for her assistance with data collection. We are also grateful to Agnese Morganti for kindly providing the photograph depicting a subject wearing the EEG net.

## Author contributions

Conceptualization: D.G., G.B.; Methodology: D.G., G.B.; Investigation: D.G., D.B.; Data curation: D.G.; Formal analysis: D.G., M.B., A.F., R.B., D.B.; Visualization: D.G.; Supervision: G.B.; Resources: G.B.; Writing—original draft: D.G., G.B.; Writing—review and editing: All authors.

## Competing interests

The authors declare no competing interests.

## Additional information

**Supplementary information** The online version contains supplementary material available at <https://doi.org/10.1038/s42003-025-08480-3>.

**Correspondence** and requests for materials should be addressed to Giulio Bernardi.

**Peer review information** *Communications Biology* thanks Bastien Lechat and the other, anonymous, reviewers for their contribution to the peer review of this work. Primary Handling Editors: Enzo Tagliazucchi and Jasmine Pan. A peer review file is available.

**Reprints and permissions information** is available at <http://www.nature.com/reprints>

**Publisher’s note** Springer Nature remains neutral with regard to jurisdictional claims in published maps and institutional affiliations.

**Open Access** This article is licensed under a Creative Commons Attribution-NonCommercial-NoDerivatives 4.0 International License, which permits any non-commercial use, sharing, distribution and reproduction in any medium or format, as long as you give appropriate credit to the original author(s) and the source, provide a link to the Creative Commons licence, and indicate if you modified the licensed material. You do not have permission under this licence to share adapted material derived from this article or parts of it. The images or other third party material in this article are included in the article’s Creative Commons licence, unless indicated otherwise in a credit line to the material. If material is not included in the article’s Creative Commons licence and your intended use is not permitted by statutory regulation or exceeds the permitted use, you will need to obtain permission directly from the copyright holder. To view a copy of this licence, visit <http://creativecommons.org/licenses/by-nc-nd/4.0/>.